university of groningen

University Medical Center Groningen

University of Groningen

Charge transport and trap states in lead sulfide quantum dot field-effect transistors

Nugraha, Mohamad Insan

IMPORTANT NOTE: You are advised to consult the publisher's version (publisher's PDF) if you wish to cite from it. Please check the document version below.

Document Version
Publisher's PDF, also known as Version of record

Publication date:
2017

Link to publication in University of Groningen/UMCG research database

Citation for published version (APA):
Nugraha, M. I. (2017). *Charge transport and trap states in lead sulfide quantum dot field-effect transistors*. [Thesis fully internal (DIV), University of Groningen]. University of Groningen.

Copyright
Other than for strictly personal use, it is not permitted to download or to forward/distribute the text or part of it without the consent of the author(s) and/or copyright holder(s), unless the work is under an open content license (like Creative Commons).

The publication may also be distributed here under the terms of Article 25fa of the Dutch Copyright Act, indicated by the “Taverne” license. More information can be found on the University of Groningen website: https://www.rug.nl/library/open-access/self-archiving-pure/taverne-amendment.

Take-down policy
If you believe that this document breaches copyright please contact us providing details, and we will remove access to the work immediately and investigate your claim.

Downloaded from the University of Groningen/UMCG research database (Pure): http://www.rug.nl/research/portal. For technical reasons the number of authors shown on this cover page is limited to 10 maximum.

Download date: 29-04-2025

Chapter 6

Strain-Modulated Charge Transport in Flexible PbS Quantum Dot Field-Effect Transistors

This chapter presents a study on the effect of mechanical strain on the charge transport properties in flexible PbS quantum dot field-effect transistors (QD-FETs). By applying compressive strain, the mobility is improved up to 45% at 2% strain, whereas a decrease of the mobility is observed with the application of tensile strain. The change of the mobility in the strained devices is attributed to the decrease/increase of the inter-QD distance due to the bending of the capping ligands. Moreover, strain is also found to affect the carrier traps in the devices as indicated from the modulated threshold voltages, because of the change of inter-QD transfer integral. From the analysis of the applied strain versus ligand length, a certain strain direction results in the activation of the ligand chains leading to the increase of the tunnelling barrier potential in the QD films.

M. I. Nugraha, H. Matsui, S. Watanabe, T. Kubo, R. Hausermann, S. Z. Bisri, M. Sytnyk, W. Heiss, M. A. Loi, J. Takeya, *Adv. Electron. Mater.* **2017**, 3, 1600360.

6.1 Introduction

Extensive progresses in understanding charge carrier transport in PbS semiconducting colloidal quantum dots (QDs) have provided hope to exploit this class of materials for low-temperature processed electronic and optoelectronic devices. Due to their solution processability, PbS QDs are compatible with solution processable fabrication methods such as spin-coating, dip-coating, ink-jet printing, etc.[1–6] This solution processability, combined with low temperature processing, opens up opportunities to use this material to fabricate electronic and optoelectronic devices on flexible plastic substrates.[7,8]

As the active materials are deposited onto flexible substrates, bending, folding, or stretching of the substrates is able to induce mechanical strain on the active layer which influences the characteristics of the fabricated devices. Recently, mechanical strain effects have been intensively investigated on organic semiconductor thin film transistors (TFTs).[9–11] The application of compressive strain on pentacene films has allowed improving the film conductivity and carrier mobility in the TFT devices as a consequence of reduced molecular spacing. Oppositely applied strain produces increased molecular spacing which leads to the decrease of the carrier mobility.[10–13] Meanwhile, the effect of mechanical strain on lead chalcogenide QD devices, particularly in field-effect transistors (FETs), is still poorly investigated. As the bulk moduli of organic ligands has been reported to be lower than the QD cores,[14,15] the introduction of mechanical strain is expected to have a great impact on the properties of the devices, with the potential to improve carrier mobility in this system. Therefore, the effect of strain on the electrical properties of QD-FETs needs to be addressed to further understand their physical properties and to strengthen the applicability of QDs for diverse applications.

In this chapter, we report a study of the effect of mechanical strain on the electrical characteristics of PbS FETs. As a gate dielectric, we use an ion gel, which is able to accumulate high carrier concentration leading to electron mobility as high as 2.1 $cm^2V^{-1}s^{-1}$. Upon the application of compressive strain, we observed an improvement in the source-drain current, which leads to an increase in the electron mobility up to 45% at 2% strain. This improvement is associated to the reduced barrier length between QDs due to the bending of crosslinking ligands. In the opposite strain direction, we observed a reduction in the electron mobility which is an indication of the increase of the QD distance. Interestingly, we found that the change in the electron mobility is followed by the variation in the threshold voltages of the devices depending on the direction of the strain. The decreased threshold voltages as the compressive strain is applied can be attributed to the increase of the transfer integral between the QD arrays, which results in a more efficient trap filling, thus reducing carrier trapping. Meanwhile,

the increased carrier traps can be responsible for the increase of the threshold voltages with the application of tensile strain. Furthermore, the observed larger effect during the application of tensile strain than that with compressive strain can be associated to the increase of barrier potential due to the activation of one or more ligand chains.

6.2 PbS QD-FETs on flexible substrates

To perform strain effect measurement on the PbS QD films, flexible PbS QD-FETs were fabricated using polyethylene naphthalate (PEN) as a substrate. As crosslinking ligands, 1,2-ethanedithiol (EDT) was used to replace the native oleic acid ligands on the QD surfaces, which improves the conductivity of the semiconducting films. In the devices, an ion gel derived from a mixture of the ionic liquid: 1-hexyl-3-methyl imidazolium bis(trifluoromethanesulfonyl)imide (HMIM-TFSI) and the gelling polymer, poly(vinylidene fluoridehexafluoro propylene) (PVDF-HFP) was employed as the gate dielectric. This mixture allows obtaining a solid gate dielectric film which is easy to handle and suitable for electronic devices fabricated on plastic substrate. The ion gel is used to accumulate high charge carrier concentration at the dielectric/semiconductor interface, which can effectively fill the carrier traps in the QD films. As a result of the effective trap filling, ion gel has been demonstrated as a promising gate dielectric that enables good performing PbS QD-FETs with high electron mobility of 2 $cm^2V^{-1}s^{-1}$.[16] Figure 6.1 (a) shows the final configuration of bottom contact top gate PbS QD-FETs fabricated on PEN substrate. In the devices, Au is used as source, drain, and gate electrode. The flexibility of the fabricated devices is displayed in Figure 6.1 (b).

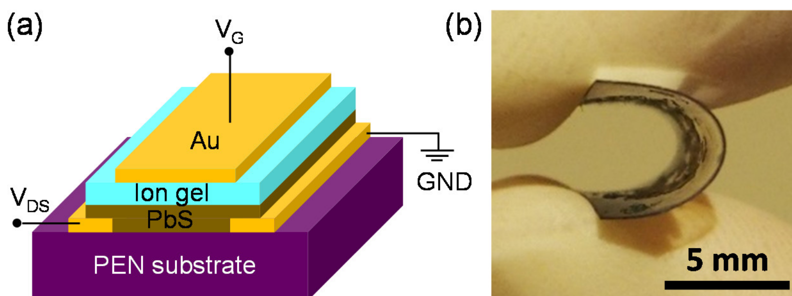

Figure 6.1 (a) Device structure, (b) photograph of PbS QD-FETs on flexible substrate.

The transfer characteristics of the fabricated devices in pristine condition (without applying strain) are shown in Figure 6.2 (a). The devices show a small hysteresis (< 1.3 V) in the transfer curves, indicating that the ion gel provides good

protection for the devices against bias stress and an effective filling of the traps.[17] Importantly, the devices show clear current modulation with very low operation voltage (<2 V), which is promising for future low energy consuming solution processable electronic devices. In addition, a weak hole current in the negative gate voltage is also measured indicating the ambipolarity of the devices. However, since the hole current is much lower than the electron current and quite close to the level of the gate leakage current, the investigation of the strain effect in this study is focused on the electron transport.

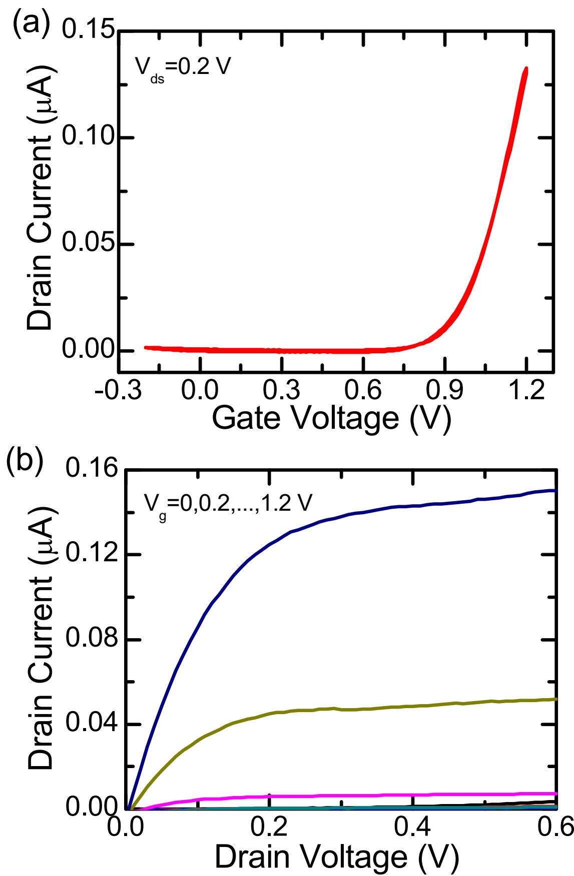

Figure 6.2 (a) I_{ds}-V_g transfer and (b) I_{ds}-V_{ds} output characteristics of PbS QD-FETs with HMIM-TFSI ion gel gating on PEN substrate.

The capacitance of the ion gel film (C_i) is as high as 2.7 μF/cm^2 at 10 Hz, allowing a very low threshold voltage of 0.9 V in the devices. The sweeping speed used for the FET measurements was 100 mV/s. In the devices, the channel length

was designed to be 150 μm to minimize the effect of contact resistance. Moreover, a channel width of 70 μm was used to avoid localized surface morphology defects formed during film deposition as well as during ligand exchange, which may obscure the effect of mechanical strain. The electron linear mobility extracted from the transfer characteristics in Figure 6.2 (a) is as high as 2.1 $cm^2V^{-1}s^{-1}$. It is important to note that this very high electron mobility is achieved in the devices fabricated on plastic substrate. In addition, the output characteristics shown in Figure 6.2 (b) indicate that the devices do not show any contact limitation at low drain voltage. Moreover, the clear saturation profiles confirm that the fabricated FETs are well performing.

6.3 Strain effect on flexible PbS QD-FETs

The fabrication of PbS QD-FETs on flexible plastic substrate allows applying compressive and tensile strain on the devices, continuously up to 2% without breaking the devices. The schematic of the application of compressive and tensile strain is shown in Figure 6.3. The radius of curvature of the samples upon the application of strain is given as,[18,19]

$$R = \frac{l}{2\pi\sqrt{\frac{dl}{l} - \frac{\pi^2 h^2}{12 l^2}}} \tag{6.1}$$

where *h*, *l*, and *dl* are the total thickness, the initial length, and the change of length of the samples, respectively. The strain can be simply estimated from $\varepsilon=(h/2R)\cdot 100\%$.[18,19]

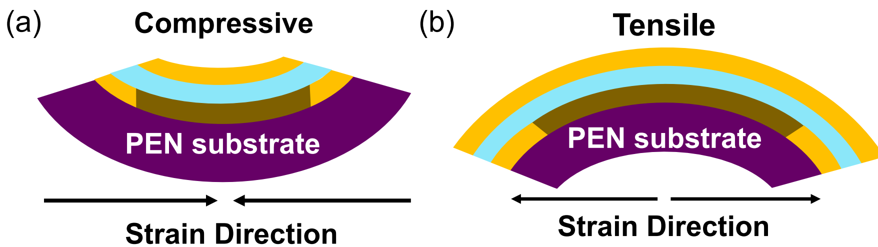

Figure 6.3 Schematic of (a) compressive (bent downward) and (b) tensile strain (bent upward) applied on the devices.

At first, the surface morphology characterization of the PbS QD films was performed to investigate the presence of cracks on the films after the application of strain. Figure 6.4 shows the AFM images of the PbS QD films on PEN substrate with different strain magnitudes. Obviously, no significant change is observed on

the PbS films indicating the absence of cracks after applying compressive and tensile strain up to 2%.

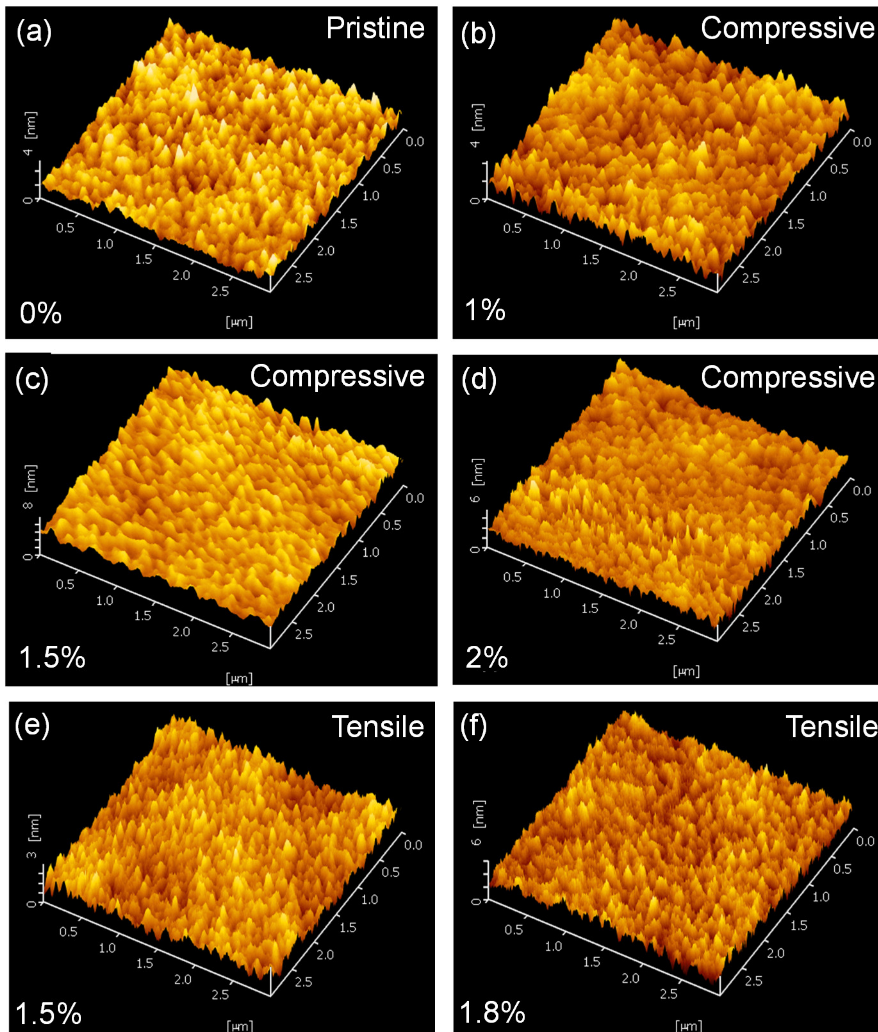

Figure 6.4 Surface morphology of the PbS films with (a) no strain and compressive strain of (b) 1%, (c) 1.5%, and (d) 2%. AFM images of the PbS films with tensile strain of (e) 1.5% and (f) 1.8%.

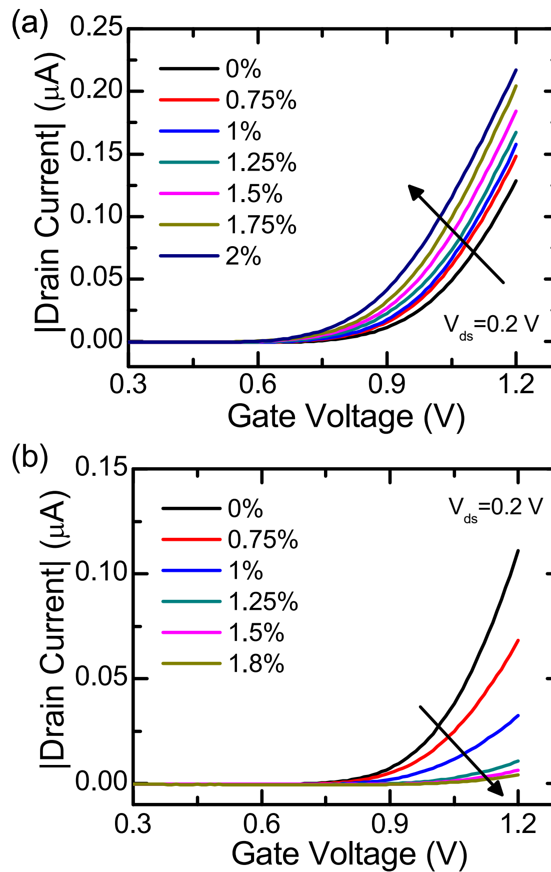

Figure 6.5 I_{ds}-V_g transfer characteristics with the application of (a) compressive and (b) tensile strain.

Figure 6.5 (a) presents the transfer characteristics of the devices under several static compressive strains. The applied compressive strain is started from 0.75% up to 2% with a strain interval of 0.25%. An improvement in the on-current of the devices is measured when the compressive strain is applied on the devices. Meanwhile, no significant change is observed in the off-current of the devices with the application of the strain as shown in Figure 6.6 (a). Furthermore, the improvement of the on-current is also followed by the shifting of the transfer curve towards more negative voltages, i.e, showing a reduced threshold voltage as displayed in Figure 6.5 (a) and 6.6 (a). Importantly, the variation of the transfer curve upon the application of compressive strain is reversible, demonstrating that the devices are still elastic after the strain is applied and that the current increase is not caused by its drifting. When the opposite strain direction (tensile strain) is applied on the devices, the decrease of the on-current is observed. The transfer

characteristics measured after the application of the tensile strain are displayed in Figure 6.5 (b) and 6.6 (b). In addition, we also observed the shift of the transfer curve towards more positive voltages, thus an increased threshold voltage.

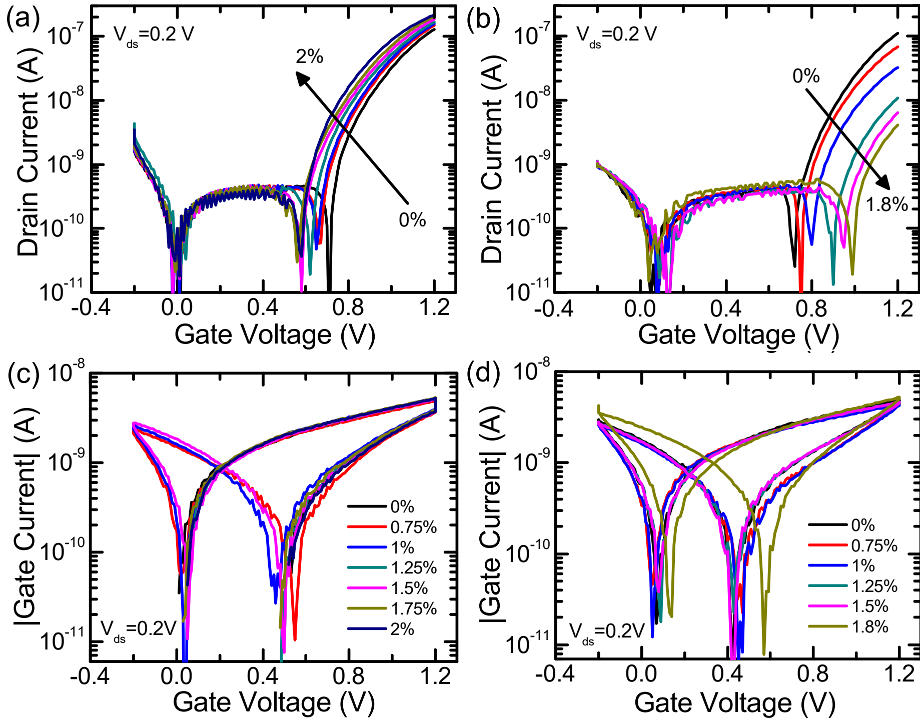

Figure 6.6 Semi-logarithmic scale of I_{ds}-V_g transfer characteristics in the devices after the application of (a) compressive and (b) tensile strain. Semi-logarithmic scale of gate leakage I_g-V_g characteristics in the devices after the application of (c) compressive and (d) tensile strain.

To have a confirmation that the variation of the on-current is not caused by changes in the dielectric properties of ion gel, the gate leakage I_g-V_g characteristics of the devices under several applied mechanical strain were measured, as displayed in Figure 6.6 (c) and (d). The measurements confirm the absence of significant changes in the gate leakage characteristics indicating that the carrier density, thus the capacitance of the ion gel, is not influenced by the application of strain.

To have better description about the influence of the mechanical strain on the electrical characteristics of the devices, the electron mobility in the devices is extracted for each strain condition. Figure 6.7 shows the electron mobility versus strain. Under compressive strain (grey region), the electron mobility increases

with increasing strain. These results are attributed to the reduced barrier length, thus the reduction of the QD-interspacing. At 2% strain (R=3.1 mm), an improvement in the electron mobility up to 45% is observed resulting in the mobility value of 3 $cm^2V^{-1}s^{-1}$. To date, the electron mobility is the highest reported value achieved in PbS QD-FETs fabricated on flexible plastic substrate. Similar to the current-voltage characteristics, the variation of mobility is reversible in the range of the applied strain, which confirms that the devices are still elastic. With given mechanical strain up to 2%, no cracks are observed on the PbS films as referred to Figure 6.4.

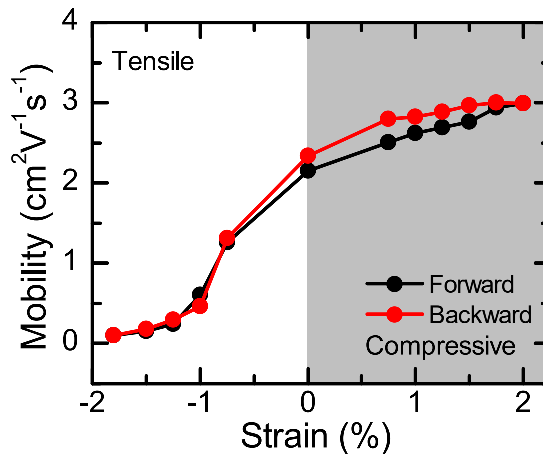

Figure 6.7 Electron mobility as compressive and tensile strain are applied.

In the region of the applied tensile strain, the decrease of the electron mobility is observed with increasing the strain magnitude as shown in Figure 6.7 (white region). These results can be ascribed to the increase of the barrier length (longer inter-QD distance) when the tensile strain is applied. The variation of the inter-QD distance by applying external pressure was reported in PbS colloidal quantum dots.[14,15] In this system, uniaxial compressive pressure results in a red shift of the excitonic peak absorption. Due to higher bulk modulus of the QD cores than that of the ligands, this shift can be mainly associated to the reduced particle spacing due to the bending of the ligands. The application of compressive strain on organic semiconductor FETs has also been reported to lead to improvement of carrier mobility due to reduced molecular spacing. The introduction of tensile strain in organic FETs results in an increased molecular spacing leading to reduced charge carrier mobility.[11,13] For organic TFTs, it has also been proposed that suppressed molecular vibration can be a possible origin of the increased charge carrier mobility.[20]

6.4 Traps and barrier potential in strained devices

The increase of the electron mobility by applying compressive strain in Figure 6.7 can also be associated with the reduction of the trap density in the devices. In quantum dot solids, the charge carrier transport mechanism is generally governed by quantum tunnelling of charge carriers between QDs. This process strongly depends on the exchange coupling energy (β), which can be written as,[3]

$$\beta = \hbar \exp\left\{-2\left(2m^* E_b / \hbar^2\right)^{1/2} d\right\} \tag{6.2}$$

where $\hbar$, m^*, and E_b are reduced *Planck* constant, the effective mass of carriers, and barrier potential height, respectively. The distance between QDs, which is proportional to the length of the ligands, is given by *d*. When compressive strain is applied, the bending of the crosslinking ligands leads to the reduced inter-QD distance, thus improving the exchange coupling energy. This increased exchange coupling energy will, in turn, reduce the carrier traps near the QD band-edge as indicated in the schematics reported in Figure 6.8.

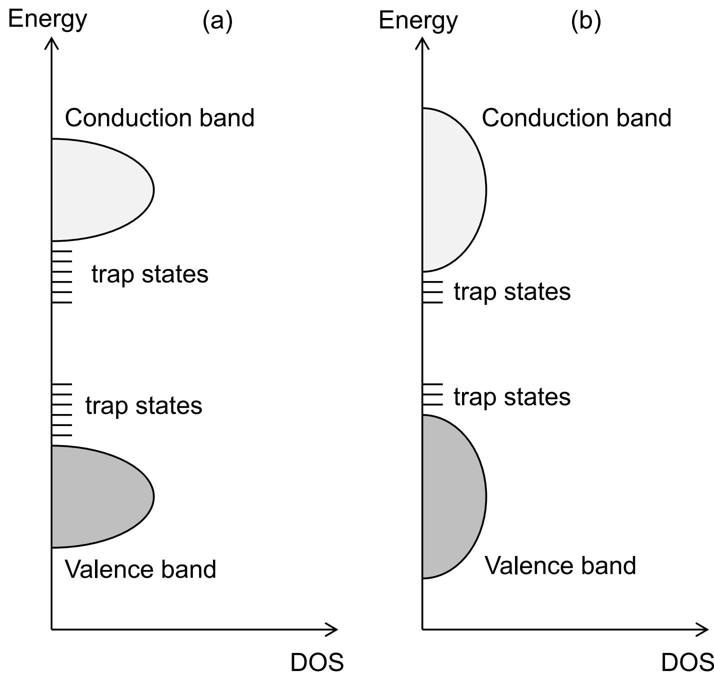

Figure 6.8 Schematics of the density of states (DOS) (a) without strain and (b) with compressive strain. The bandwidth increases due to the increased transfer integral.

Conversely, the application of tensile strain will result in the reduction of the exchange coupling energy. As a consequence, some carrier traps will be introduced in the band edge of quantum dots. The analysis on this trap modulation is also supported by the observed threshold voltage shifts upon the application of the strain as shown in Figure 6.9. As compressive strain increases, the threshold voltage decreases indicating a lower energy for electron accumulation, which is related to the reduction of the traps in the devices. When tensile strain is applied, the increase of the threshold voltage in the devices is observed. This threshold voltage shift explains the increase of energy for electron accumulation, which can be attributed to the increased number of carrier traps. This fluctuation of density of states due to the change of the exchange coupling bandwidth was previously observed in organic semiconductors. [21–24]

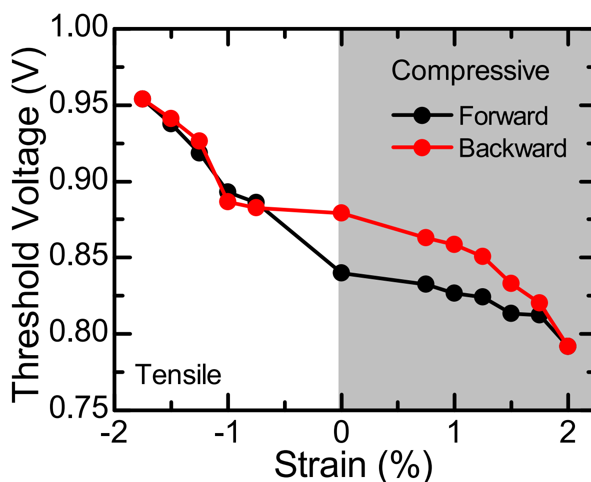

Figure 6.9 Threshold voltage of the devices with the application of compressive and tensile strain.

Interestingly, a non-fully-symmetrical profile in the variation of the device characteristics by comparing the conditions between compressive and tensile strain is observed, as referred to Figure 6.7 and 6.9. At this point, the effect of tensile strain on the device characteristics is larger than that with compressive strain. This result can be explained by the induction of a barrier potential with the introduction of tensile strain. To understand this effect, the change of the inter-QD distance due to the applied strain (ε) is firstly estimated using equation $\Delta x = x\varepsilon$, where x is the distance between the center of mass of QDs. When compressive strain is applied, the inter-QD distance is the only parameter changed due to the bending of the ligands. When the tensile strain is applied on the QD films, the inter-QD distance is increased by bending the crosslinking organic ligands. Due

to this bending, at some points, one of thiol end groups on the QD surfaces can also become active as demonstrated in Figure 6.10 (a). These active thiols may increase the barrier potential between QDs and result in the reduced number of the ligands interconnecting the PbS QDs, thus reducing the tunnelling probability between QDs as indicated in equation (6.2). In addition, the change of the ligand dielectric constant when the ligands are stretched can be another possible origin for the change of barrier potential height.

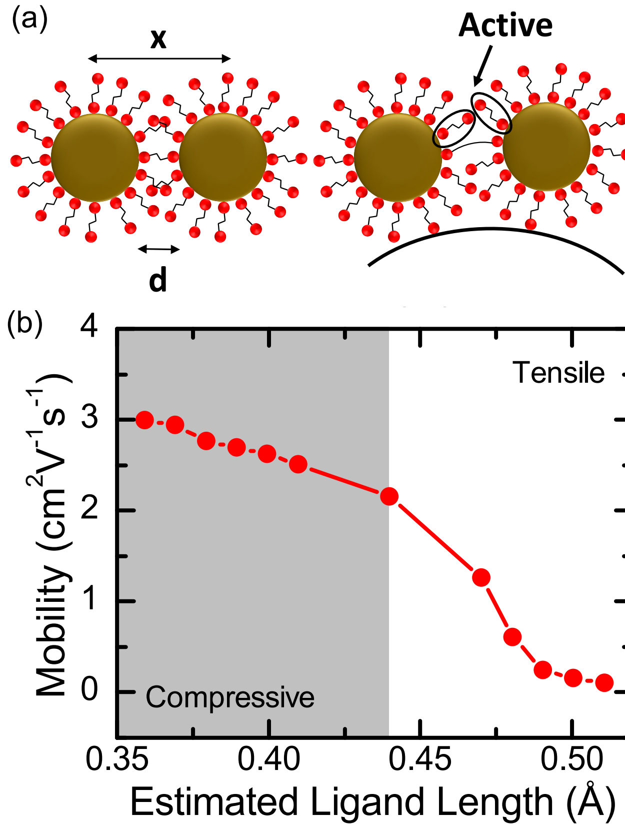

Figure 6.10 (a) Unbound (active) ligand chains during the application of tensile strain. (b) The electron mobility as a function of the ligand length when compressive and tensile strain are applied.

To estimate the change of the tunnelling barrier potential (E_b) in the PbS QD films, we use Wentzel–Kramers–Brillouin (WKB) approximation $\beta_e=(2m^*E_b/\hbar^2)^{1/2}$.[25] The tunnelling decay constant (β_e) can be calculated from the gradient of the curve of the calculated mobility versus estimated ligand length ($d+\Delta x$). From Figure 6.10 (b), β_e is a factor of 5 higher in the regime with tensile

strain application (β_e=4.3/Å) than that with compressive strain (β_e=0.86/Å) indicating the increase of barrier potential by referring to the WKB approximation. These results are in line with the previous reports showing that HOMO-LUMO gap for unbound (active) alkane chains is as high as 8-10 eV which is about 2 eV higher than that for bound (non-active) ligands. The lower barrier potential in the ligands bound on the QD surfaces can be attributed to the hybridization of the organic ligand chains and the orbitals of the QD surface atoms, which can introduce some density of states in the molecular junction.[25]

6.5 Conclusion

We have conducted a study of the effect of mechanical compressive and tensile strain on the electrical characteristics of PbS QD-FETs. After the application of the mechanical strain, the electron mobility was improved up to 45% (mobility of 3 $cm^2V^{-1}s^{-1}$) at 2% compressive strain, which is attributed to the reduced inter-QD distance due to the bending of ligands. The inter-QD distance can be increased by applying tensile strain, which results in a reduced electron mobility. The variation of the electron mobility by applying mechanical strain was followed by a variation of the threshold voltage of the devices. With the application of compressive strain, the threshold voltage increases due to the increased transfer integral between the QD arrays and reduced carrier traps. In the opposite strain direction, carrier traps are induced by reducing the exchange coupling energy, which in turn leads to a decreased transfer integral of the QD arrays. The application of tensile strain gave rise to a larger effect than that of compressive strain. This finding can be associated to an increase of the barrier potential due to the activation of some of the thiol ligands. These results provide fundamental understanding of the effect of mechanical forces on PbS films which can enhance and broaden the applicability of these materials for flexible cheap solution processable electronic devices and also open new prospective towards the fabrication of mechanical force sensors.

6.6 Methods

Device Fabrication. Polyethylene naphthalate (PEN) with thickness of 125 μm was used as a substrate. Before use, the substrate was annealed at 150°C for 3 h on a hot plate to remove residual monomer on the PEN surfaces. The substrate was cleaned with isopropanol for 10 min and dried with nitrogen. Cr and Au (10 nm/30 nm) were then evaporated on the clean PEN substrate as source-drain contacts.

PbS quantum dots were synthesized following a method previously reported in literature.[26] The deposition of the PbS semiconducting thin film was done by

spin coating 10 mg/mL of the oleic acid-capped QD solution in chloroform. To improve the film conductivity, the long-alkyl-chain oleic acid ligands were replaced by shorter organic molecules, 1,2-ethanedithiol (EDT) with concentration of 1% v/v in acetonitrile. The film deposition and ligand exchange (LE) were done using layer-by-layer spin coating procedures for 7 times to ensure complete LE process. After each LE process, the film was cleaned with pure acetonitrile to remove old native ligands. The devices were annealed at 120°C for 20 min to remove residual solvents and promote stronger coupling between QDs.

Ion gel based on 1-hexyl-3-methyl-imidazolium bis(trifluoromethane sulfonyl) imide (HMIM-TFSI) ionic liquid was used as gate dielectric. To prepare the solution of ion gel, 80 mg of poly(vinylidene fluoride hexa- fluoropropylene) (PVDF-HFP) pellets was first dissolved in 1 mL dimethylformamide. The solution was stirred at 60°C overnight. 20 mg of HMIM-TFSI ionic liquid was then added into the PVDF-HFP solution and stirred at room temperature for 3 h. The ion gel solution was then spin-coated on the PbS film and annealed at 90°C for 2 h. Finally, Au with thickness of 50 nm was evaporated on the top of the ion gel film as top gate electrode. All device fabrication was performed in an N_2-filled glove box

Device Measurement and Strain Effect Experiment. The FET electrical characteristics were measured using an Agilent B1500A semiconductor parameter analyser connected to a probe station in an N_2-filled glove box. For strain effect measurement, the devices were stressed using strain measurement apparatus. The change of the device length was measured by using a calliper and then used in equation (6.1) to further calculate the strain. The initial ligand length (without strain) was estimated using the Gaussian software. Before performing the electrical transport measurement, we waited for 10 minutes after changing each level of strain to relax some slow ionic migration of the ion gel.

6.7 References

[1] M. I. Nugraha, R. Häusermann, S. Z. Bisri, H. Matsui, M. Sytnyk, W. Heiss, J. Takeya, M. A. Loi, *Adv. Mater.* **2015**, *27*, 2107.
[2] D. M. Balazs, D. N. Dirin, H.-H. Fang, L. Protesescu, G. H. ten Brink, B. J. Kooi, M. V. Kovalenko, M. A. Loi, *ACS Nano* **2015**, *9*, 11951.
[3] D. V Talapin, J.-S. Lee, M. V Kovalenko, E. V Shevchenko, *Chem. Rev.* **2010**, *110*, 389.
[4] M. V Kovalenko, M. Scheele, D. V Talapin, *Science* **2009**, *324*, 1417.
[5] M. V Kovalenko, M. I. Bodnarchuk, J. Zaumseil, J.-S. Lee, D. V Talapin, *J. Am. Chem. Soc.* **2010**, *132*, 10085.
[6] E. J. D. Klem, H. Shukla, S. Hinds, D. D. MacNeil, L. Levina, E. H. Sargent, *Appl. Phys. Lett.* **2008**, *92*, 212105.
[7] F. S. Stinner, Y. Lai, D. B. Straus, B. T. Diroll, D. K. Kim, C. B. Murray, C. R. Kagan, *Nano Lett.* **2015**, *15*, 7155.
[8] J.-H. Choi, H. Wang, S. J. Oh, T. Paik, P. Sung, J. Sung, X. Ye, T. Zhao, B. T. Diroll, C. B. Murray, C. R. Kagan, *Science.* **2016**, *352*, 205.
[9] S. H. Nam, P. J. Jeon, S. W. Min, Y. T. Lee, E. Y. Park, S. Im, *Adv. Funct. Mater.* **2014**, *24*, 4413.
[10] P. Cosseddu, G. Tiddia, S. Milita, A. Bonfiglio, *Org. Electron.* **2013**, *14*, 206.
[11] T. Sekitani, Y. Kato, S. Iba, H. Shinaoka, T. Someya, T. Sakurai, S. Takagi, *Appl. Phys. Lett.* **2005**, *86*, 1.
[12] T. Sekine, K. Fukuda, D. Kumaki, S. Tokito, *Jpn. J. Appl. Phys.* **2015**, *54*, 04DK10.
[13] K. Fukuda, K. Hikichi, T. Sekine, Y. Takeda, T. Minamiki, D. Kumaki, S. Tokito, *Sci. Rep.* **2013**, *3*, 2048.
[14] K. Bian, B. T. Richards, H. Yang, W. Bassett, F. W. Wise, Z. Wang, T. Hanrath, *Phys. Chem. Chem. Phys.* **2014**, *16*, 8515.
[15] K. Bian, A. K. Singh, R. G. Hennig, Z. Wang, T. Hanrath, *Nano Lett.* **2014**, *14*, 4763.
[16] S. Z. Bisri, C. Piliego, M. Yarema, W. Heiss, M. A. Loi, *Adv. Mater.* **2013**, *25*, 4309.
[17] Y. Zhang, Q. Chen, A. P. Alivisatos, M. Salmeron, *Nano Lett.* **2015**, 150625084251003.
[18] S. Il Park, J. H. Ahn, X. Feng, S. Wang, Y. Huang, J. A. Rogers, *Adv. Funct. Mater.* **2008**, *18*, 2673.
[19] S. P. Timoshenko, J. M. Gere, in *Theory Elastic Stab.*, McGraw Hill, New York, **1961**, p. Ch 2 and 9.
[20] T. Kubo, R. Häusermann, J. Tsurumi, J. Soeda, Y. Okada, Y. Yamashita, N. Akamatsu, A. Shishido, C. Mitsui, T. Okamoto, S. Yanagisawa, H. Matsui, J. Takeya, *Nat. Commun.* **2016**, *7*, 11156.
[21] G. Lu, J. Blakesley, S. Himmelberger, P. Pingel, J. Frisch, I. Lieberwirth, I. Salzmann, M. Oehzelt, R. Di Pietro, A. Salleo, N. Koch, D. Neher, *Nat. Commun.* **2013**, *4*, 1588.
[22] A. Troisi, *Mol. Simul.* **2006**, *32*, 707.
[23] A. Troisi, G. Orlandi, *J. Phys. Chem. A* **2006**, *110*, 4065.
[24] A. Troisi, G. Orlandi, *Phys. Rev. Lett.* **2006**, *96*, 1.
[25] Y. Liu, M. Gibbs, J. Puthussery, S. Gaik, R. Ihly, H. W. Hillhouse, M. Law, *Nano*

Lett. **2010**, *10*, 1960.
[26] M. A. Hines, G. D. Scholes, *Adv. Mater*. **2003**, *15*, 1844.